Mass Spectrometry Imaging of the Hypoxia Marker Pimonidazole in a Breast Tumor Model

Nadine E. Mascini[1], Menglin Cheng[2], Lu Jiang[2], Asif Rizwan[2], Helen Podmore[3], Dhaka R. Bhandari[4], Andreas Römpp[5], Kristine Glunde[2,6,*], Ron M.A. Heeren[1,7,*]

[1] FOM Institute AMOLF, 1098 XG Amsterdam, The Netherlands.

[2] The Johns Hopkins University In Vivo Cellular and Molecular Imaging Center, Division of Cancer Imaging Research, The Russell H. Morgan Department of Radiology and Radiological Science, The Johns Hopkins University School of Medicine, Baltimore, MD 21205, USA.

[3] Thermo Fisher Scientific, Stafford House, Boundary Way, Hemel Hempstead, Herts, United Kingdom.

[4] TransMIT GmbH · TransMIT Center for Mass Spectrometric Developments, Schubertstrasse 60, 35392 Giessen, Germany.

[5] Institute of Inorganic and Analytical Chemistry, Justus Liebig University Giessen, Schubertstrasse 60, 35392 Giessen, Germany.

[6] Sidney Kimmel Comprehensive Cancer Center, The Johns Hopkins University School of Medicine, Baltimore, MD 21231, USA.

[7] The Maastricht Multimodal Molecular Imaging institute (M4I), 6229 ER Maastricht, The Netherlands.

ABSTRACT: Although tumor hypoxia is associated with tumor aggressiveness and resistance to cancer treatment, many details of hypoxia-induced changes in tumors remain to be elucidated. Mass spectrometry imaging (MSI) is a technique that is well suited to study the biomolecular composition of specific tissue regions, such as hypoxic tumor regions. Here, we investigate the use of pimonidazole as exogenous hypoxia marker for matrix-assisted laser desorption/ionization (MALDI) MSI. In hypoxic cells, pimonidazole is reduced and forms reactive products that bind to thiol groups in proteins, peptides and amino acids. We show that a reductively activated pimonidazole metabolite can be imaged by MALDI-MSI in a breast tumor xenograft model. Immunohistochemical detection of pimonidazole adducts on adjacent tissue sections confirmed that this metabolite is localized to hypoxic tissue regions. We used this metabolite to image hypoxic tissue regions and their associated lipid and small molecule distributions with MALDI-MSI. We identified a heterogeneous distribution of 1-methylnicotinamide and acetylcarnitine, which mostly co-localized with hypoxic tumor regions. As pimonidazole is a widely used immunohistochemical marker of tissue hypoxia, it is likely that the presented direct MALDI-MSI approach is also applicable to other tissues from pimonidazole-injected animals or humans.

Tumor hypoxia, caused by abnormal tumor vasculature, is associated with tumor aggressiveness and resistance to cancer treatment.[1] Tissue regions with a partial oxygen pressure (pO_2) below 10 mmHg are typically considered hypoxic, but the degree of hypoxia can vary considerably inside and between different tumors.[2] Hypoxia is found in many solid tumors and triggers a complex response that involves many different molecular pathways. These pathways influence cellular processes such as apoptosis, angiogenesis, proliferation and anaerobic metabolism. Understanding the hypoxia-induced changes in tumors is essential for the development of more effective cancer treatment. This requires the development of innovative techniques that can image hypoxia and its associated biomolecular changes.

Given the importance of hypoxia, many techniques have been developed for measuring tumor oxygenation. These techniques include direct pO_2 measurement with polarographic oxygen electrodes or fiber optic probes, magnetic resonance and other imaging techniques.[1,3] In recent years, endogenous markers such as hypoxia-inducible factor 1 (HIF-1), carbonic anhydrase IX (CAIX), glucose transporter 1 (GLUT1), C-X-C chemokine receptor type 4 (CXCR4), vascular endothelial growth factor (VEGF) and insulin-like growth factor 1 receptor (IGF1R) have been reported for hypoxia imaging.[1,4] However, the expression of these markers is not directly linked to the oxygenation status of the tissue and they are therefore often referred to as hypoxia-related markers.[1]

The exogenous 2-nitroimidazole hypoxia markers were originally designed as radiosensitizers, but the observation that they were activated and retained in viable hypoxic cells with an oxygen dependence similar to that of radioresistance led to the development of this class of molecules as hypoxia markers.[5-7] Several methods exist for the detection of 2-nitroimidazole adducts, including positron emission tomography (PET), single photon emission computed tomography (SPECT), magnetic resonance spectroscopy (MRS) and immune-histochemical assays.[8] Antibody-based detection methods have the advantage that hypoxia can be imaged on a cellular level. The spatial distribution of hypoxia as detected with antibodies recognizing 2-nitroimidazoles can be compared with high spatial detail to other markers of tumor biology.[9,10] A disadvantage of immunohistochemical assays is that they

are targeted assays with limited multiplexing capability, hence only known targets can be studied and only a small number of proteins can be detected at the same time.

Matrix-assisted laser desorption/ionization (MALDI) mass spectrometry imaging (MSI) can image hundreds of analytes directly from tissue surfaces. It can visualize a wide variety of biomolecules, such as lipids, proteins, peptides and metabolites routinely at 50-100 µm spatial resolution, but recent technical developments have shown that lipids and drug compounds can be imaged with a resolution of 5-10 µm.[11-13] These characteristics make MALDI-MSI well suited to study the biomolecular make-up of hypoxic tissue regions, provided that there is an easy way of discriminating hypoxic from normoxic tissue regions.

Here we present a MALDI-MSI approach that combines the detection of the 2-nitroimidazole hypoxia marker pimonidazole, and the multiplexing capabilities of this technique to image hypoxic regions and their associated biomolecules in a single experiment.

Pimonidazole was shown to be a reliable marker of hypoxia and is approved for clinical use.[14,15] Importantly, it has favorable chemical properties for mass spectral detection such as a slightly basic piperidine side chain. Pimonidazole is reduced only under hypoxic conditions to form reactive products that bind to cellular nucleophiles, especially thiol-containing proteins. Reductive activation is inhibited at pO_2 >10 mmHg in solid tissue (half-maximal inhibition at ca. 2 mmHg).[16-18] Pimonidazole reduction depends upon nitroreductase activity; hence metabolically active cells are required for reductive metabolism of pimonidazole. Limited knowledge exists on the *in vivo* reaction products of pimonidazole.[19] Current knowledge is largely based on *in vitro* and simple *in vivo* experiments that were performed in the 1980's.[7,20-25] For these experiments a different 2-nitromidazole, misonidazole, was primarily used.

In this study, we used MALDI-MSI to study pimonidazole and its metabolism in breast cancer xenograft tissue from pimonidazole-injected mice. We detected the unreacted pimonidazole compound and several pimonidazole metabolites. Accurate mass and product ion measurements with atmospheric pressure scanning microprobe MALDI (AP-SMALDI) MSI and accurate mass liquid chromatography (LC) MS experiments were performed to analyze tumor tissue from pimonidazole-injected mice in detail. Verification was performed by immunohistochemical detection of pimonidazole adducts on adjacent tissue sections. We show that one of the detected pimonidazole metabolites is well suited as marker of hypoxia in MALDI-MSI experiments. We also present small molecules that co-localize with the hypoxic regions as detected by this pimonidazole metabolite.

EXPERIMENTAL SECTION

Preparation of breast tumors for stainings and MSI analysis. Triple-negative MDA-MB-231 breast cancer cells, obtained from the American Type Culture Collection (ATCC), were orthotopically inoculated into the mammary fat pad of athymic nude mice. Tumors were grown to 6-8 mm in diameter within about 8 weeks. 400 mg/kg of pimonidazole was injected intravenously into the tail vein. Pimonidazole, primary mouse anti-pimonidazole antibody conjugated with FITC, secondary rabbit anti-FITC antibody, and all immunohistochemical (IHC) staining reagents were purchased as a kit (HP2-100 Kit, Hypoxyprobe, Burlington, MA, USA). After 30 minutes, the mice were sacrificed, tumors were excised and embedded in gelatin. An equal mixture of Cresyl Violet and Ponceau S (0.5 mg/mL of each as final concentration), were added as fiducial markers for spatial referencing.[26] The embedded tumors were frozen in liquid nitrogen and stored at -80 °C. Four tumors were used in this study: three from pimonidazole-injected mice and one from an untreated control mouse.

During cryosectioning, tumors were divided into about ten sets of cryosections. Four 100 µm thick sections were cut for each set and stored in eppendorf tubes. Then, seven 10 µm sections were cut per set. Adjacent sections were mounted on glass slides for hematoxylin and eosin (H&E) and IHC staining and on indium-tin oxide (ITO) coated slides (Delta Technologies, Stillwater, MN, USA) for MSI analysis. Details on the H&E and IHC staining and the chemicals used in this study are available as Supporting Information. All sections analyzed originated from tissues sets 6-9 as counted from the mouse body wall to the top of the tumor, except for the sections used for metabolite extraction which originated from throughout the tumor. All sections were stored at -80 °C until analysis.

MALDI mass spectrometry. α-cyano-4-hydroxycinnamic acid (CHCA) matrix solution was prepared at a concentration of 10 mg/mL in 50% ACN (vol/vol) and 0.2% trifluoroacetic acid (TFA) in water. Pimonidazole standard solution was prepared by mixing a pimonidazole solution of 1 mg/mL in MeOH with CHCA matrix solution in a 1:1 ratio. The sample was spotted on a MALDI target plate at 0.5 µL per spot. We analyzed multiple breast tumor sections from three pimonidazole-injected mice and from one untreated control mouse. Sections were dried prior to MSI analysis. CHCA solution was sprayed onto the sections by a vibrational sprayer (ImagePrep, Bruker Daltonics, Bremen, Germany).

MALDI mass spectrometric analyses were performed on a MALDI-QTOF instrument (Synapt HDMS, Waters, UK) in positive ion mode. Quadrupole transmission was optimized for detecting pimonidazole-derived ions. MS images were acquired with a laser step size of 100 µm and with a mass range set between *m/z* 75 and 1000. Collision-induced dissociation was performed in the trap cell with a collision energy of 15-35 eV. Fragmentation spectra of pimonidazole-derived *m/z* 223.2 and endogenous tissue species were collected using on-tissue MS/MS. Pimonidazole standard solution spots were used to acquire MS and MS/MS spectra of the compound. Pimonidazole was detectable down to 0.5 pmol (mass accuracy 100 ppm). MALDI MS Images were generated using BioMap 3.8.0.4 software (Novartis, Basel, Switzerland) with $\Delta m/z = \pm 0.02$.

AP-SMALDI mass spectrometry. CHCA matrix solution was prepared at a concentration of 5 mg/mL CHCA in 50% ACN (vol/vol) and 0.2% TFA in water. Matrix solution was sprayed onto a dried tissue section using a Suncollect sprayer (SunChrom, Friedrichsdorf, Germany).

Experiments were performed using an atmospheric pressure scanning microprobe matrix-assisted laser desorption/ionization imaging source (AP-SMALDI10, TransMIT, Giessen, Germany),[27] coupled to an orbital trapping mass spectrometer (Q Exactive, Thermo Fisher Scientific, Bremen, Germany).

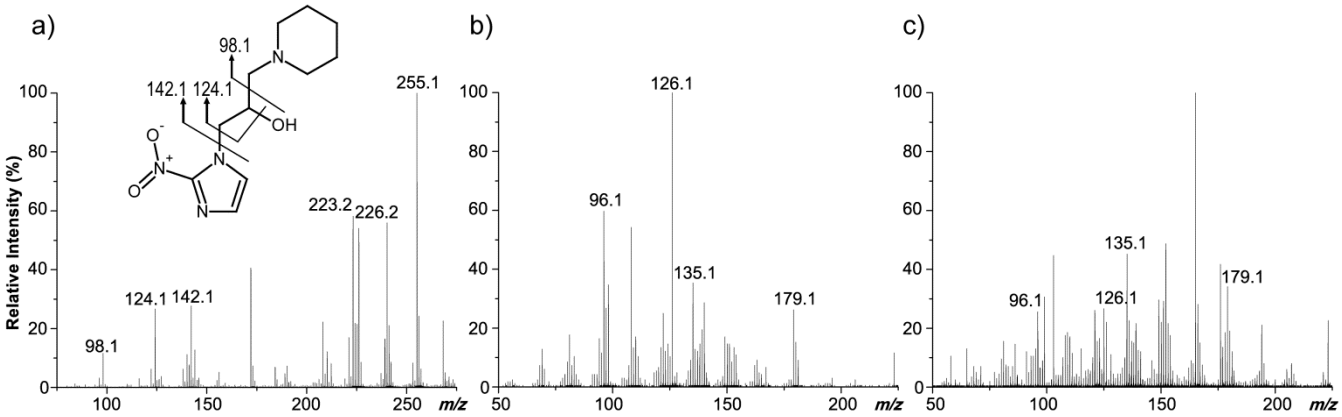

Figure 1. MALDI mass spectra of pimonidazole obtained from the pure compound and from tumor tissue from a pimonidazole-injected mouse. (a) MALDI mass spectrum of pimonidazole. Shown are the protonated parent ion at *m/z* 255.1 and its main fragments. Inset: Chemical structure of pimonidazole with characteristic fragments as determined by MS/MS. On-tissue MS/MS analysis shows that *m/z* 223.2 is a pimonidazole-derived ion. MS/MS spectra of *m/z* 223.2 from (b) pimonidazole and (c) pimonidazole-treated tissue.

MS and MS/MS data were acquired in positive ion mode. MS image size was 50 x 50 pixels, with a step size of 100 µm. Internal calibration was achieved using CHCA signals as lock masses. On-tissue MS/MS of *m/z* 223.2 was performed using higher-energy collisional dissociation (HCD) and a precursor ion isolation window of 1 Da. For HCD the normalized collision energy was set to 65%. AP-SMALDI MS images were generated with the software package Mirion[28] with Δ*m/z* = ±0.004. Spectra were analyzed with XCalibur software (Thermo Scientific).

LC-MS analysis of pimonidazole metabolites. Several 100 µm-tick tumor tissue sections, from one pimonidazole-injected and one untreated mouse, that were adjacent to sections analyzed with MSI, were used for metabolite extraction. The following extraction protocol was used: 25 mg frozen tissue was placed in pre-cooled 1.5 mL tubes, and glass beads (1 mm diameter) and 200 µL pre-cooled MeOH were added. Tissue samples were homogenized six times for 10 s, using a mini-bead beater (Biospec, Bartlesville, OK, USA), with 20 s on ice in between the homogenization rounds to avoid heating of the samples. Next, the samples were centrifuged for 5 min at 10,000g at 4°C. Supernatants were transferred to new tubes and centrifuged again for 5 min at 20,000g at 4°C to remove remaining debris. Samples were stored at -20°C until analysis. A pimonidazole solution of 100 ng/mL in MeOH was used as control sample.

High-performance liquid chromatography was performed on a Thermo Scientific Dionex Ultimate 3000 RSLC system equipped with an Accucore C18 column (100 mm x 2.1 mm, particle size 2.6 µm) at 40°C. The injection volume was 2 µL and separation was achieved using a 10 min gradient with a flow rate of 400 µL/min. Mobile phase A consisted of 10 mM ammonium acetate at pH 9.8. Mobile phase B consisted of ACN with 0.1% formic acid. This setup was connected to an Orbitrap Fusion instrument (Thermo Fisher Scientific). This mass spectrometer was operated in positive ion mode with a scan range of *m/z* 80-300. Data analysis was performed with Xcalibur and Compound Discoverer software (Thermo Scientific).

Image co-registration and correlation analysis. Image co-registration and correlation analysis were performed with Matlab software (The Mathworks Inc., Natick, MA, USA) using peak-picked and total ion count (TIC) normalized data.[29] We analyzed three sections from three different breast tumors from pimonidazole-injected mice that were imaged by the approach described above. Ion images of individual *m/z* values were co-registered to the optical image of the anti-pimonidazole stained tissue samples using the position of fiducial markers and tumor boundary, as previously described.[30] Overlap between IHC and MSI detection of pimonidazole was determined by overlaying individual ion images and the anti-pimonidazole stained images. The overlap images were constructed by using a relative threshold of 0.2 for all ion images, which means that only the 80% of pixels with the highest intensity were plotted as green dots. Correlation analysis was performed by calculating Pearson's correlation coefficients for *m/z* 223.2 with all other variables (i.e. *m/z* values), for each MSI dataset.

Identification of endogenous metabolites. Endogenous metabolites were identified from parent ion masses and fragmentation spectra. Accurate mass data (<1 ppm mass error) were obtained from on-tissue AP-SMALDI MS experiments (except for *m/z* 428.3, which was identified only from on-tissue MALDI MS/MS spectra). AP-SMALDI MS spectra were analyzed with XCalibur software. Fragmentation spectra were obtained from MALDI on-tissue MS/MS product ion acquisition and analyzed with MassLynx software (Waters, UK). LIPID MAPS (www.lipidmaps.org), the Human Metabolome Database (version 3.6, www.hmdb.ca) and MassBank (www.massbank.jp) were used to search for structures and fragmentation spectra.

RESULTS AND DISCUSSION

Detection of pimonidazole by MALDI-MS. The pimonidazole compound was readily detectable with MALDI as the protonated molecule (*m/z* 255.1). Also, several pimonidazole fragments were detected in the MS mode, with the highest intensity fragments at *m/z* 98.1, 124.1, 142.1, 223.2 and 226.2 (Figure 1a). The ions at *m/z* 98.1, 124.1 and 142.1 are fragments of the piperidine side chain.[14] Other fragments contain the imidazole ring atoms or parts of the imidazole ring. Only low intensity fragments were observed in an electrospray ionization (ESI) experiment; *m/z* 124.1 and 142.1 were detected with 100x lower intensity than *m/z* 255.1.

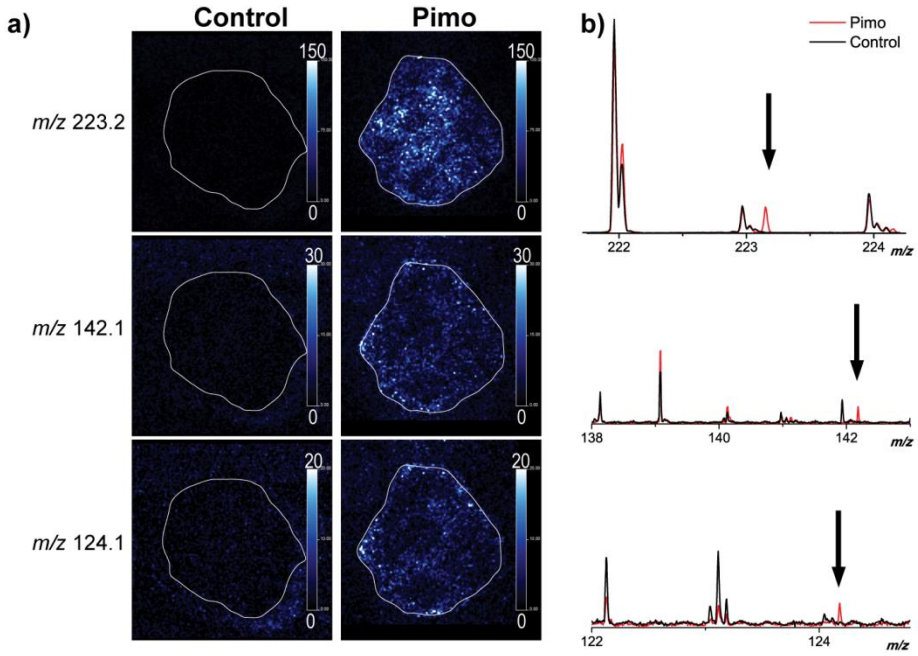

Figure 2. MALDI-MSI analysis shows the distribution of pimonidazole-derived ions in tumor tissue. (a) Pimonidazole (Pimo)-derived ions with *m/z* 124.1, 142.1 and 223.2 are solely detected in tumor tissue from pimonidazole-injected mice, and not in control tumor tissue. (b) MALDI-MSI spectra (zoom) from treated (red) and untreated (black) tumor tissue. Presence of pimonidazole-derived ions is indicated with an arrow.

The observed fragmentation can thus mainly be attributed to the desorption/ionization process used. Misonidazole, a pimonidazole analog, has an absorbance maximum at 325 nm,[7] which is close to 355 nm, the wavelength of the laser used. This might explain pimonidazole's easy fragmentation behavior in MALDI.

MALDI-MSI of pimonidazole in breast tumor xenografts. We analyzed three breast tumors from pimonidazole-injected mice and one untreated control tumor. Figure 2a shows the MS images of three detected pimonidazole-derived ions, *m/z* 124.1, 142.1 and 223.2. The protonated parent ion was also observed at *m/z* 255.1. Overlays of average spectra of pimonidazole-treated and untreated tumor tissue (Figure 2b) show the detection of these ions only in the pimonidazole-treated tumor tissue and not in the control tumor tissue. On-tissue MS/MS fragmentation of *m/z* 223.2 confirmed its pimonidazole-derived nature (Figure 1b and c). The pimonidazole-derived ions could be detected in tumor tissue from pimonidazole-injected mice down to a dose of 50 mg/kg, which was the lowest dose tested in this study (data not shown). Given the low molecular weight of pimonidazole, high mass accuracy measurements with an Orbitrap mass analyzer were performed to confirm the elemental composition of the detected ions. The predicted composition from on-tissue mass measurements matched those of the pimonidazole compound and its derivatives as listed in Table 1.

Detection of pimonidazole metabolism. It is well known that 2-nitroimidazoles are heavily metabolized *in vivo*. Under hypoxic conditions, these compounds are reduced, and after a series of steps they finally bind to cellular nucleophiles. It is estimated from *in vitro* experiments that around 20% of reductively activated 2-nitroimidazoles react with thiol containing proteins and small molecules such as glutathione.[25] The remaining 80% is subject to hydrolytic fragmentation. Several 2-nitroimidazole metabolites are described in the literature, either in *in vivo* or *in vitro* experiments.[7,20-25,31]

We searched for pimonidazole metabolites that are part of the reductive metabolism of pimonidazole. These metabolites are not generated under normoxic conditions, nor in necrotic tissue. Their confinement to hypoxic regions makes them markers of tumor hypoxia. To characterize the metabolic changes that pimonidazole undergoes in hypoxic regions, metabolites and other small molecules were extracted from treated and untreated tumor tissue, and analyzed by LC-MS.

The pimonidazole compound was included as a standard in our analysis to check for mass spectrometry-induced changes to this compound. Several species that are part of the reductive pathway with low or no abundance in the standard and untreated tumor sample were identified (Table 2 and Supporting Information Figure S-1).

Table 1. Monoisotopic mass values for pimonidazole-derived ions from tumor tissue.

Elemental composition[a]	Adduct	Exact mass	Measured accurate mass	Mass error (ppm)
$C_{11}H_{19}N_4O_3$	$[M+H]^+$	255.14517	255.14497	-0.8
$C_{11}H_{19}N_4O$	$[M]^{+,b}$	223.15534	223.15522	-0.5
$C_8H_{16}NO$	$[M]^{+,c}$	142.12264	142.12267	0.2
$C_8H_{14}N$	$[M]^{+,c}$	124.11208	124.11222	1.1

[a]Assignments are based on high mass accuracy (<3 ppm root-mean-square error). [b]Based on collision energy required to induce fragmentation. [c]Based on prediction from ESI data of pimonidazole in Metlin database.

Table 2. Pimonidazole metabolites after *in vivo* reduction of pimonidazole.

RT (min)	Measured accurate mass	Exact mass	Mass error (ppm)	Adduct	Elemental composition[d]	Proposed metabolite
7.7	201.17094	201.17099	-0.2	$[M+H]^+$	$C_9H_{21}N_4O$	Guanidine derivative
2.9	223.15528	223.15534	-0.2	$[M]^+$	$C_{11}H_{19}N_4O$	Nitrenium or related
7.7	225.17095	225.17099	-0.1	$[M+H]^+$	$C_{11}H_{21}N_4O$	Amine derivative
2.8/3.9	241.16582	241.16590	-0.3	$[M+H]^+$	$C_{11}H_{21}N_4O_2$	Hydroxylamine/ hydroxyl derivative
7.7	259.17704	259.17647	2.2	$[M+H]^+$	$C_{11}H_{23}N_4O_3$	Dihydro dihydroxy derivative
3.0	271.17639	271.17647	-0.3	$[M+H]^+$	$C_{12}H_{23}N_4O_3$	Methoxy derivative
7.7	273.19205	273.19212	-0.2	$[M+H]^+$	$C_{12}H_{25}N_4O_3$	Methoxy derivative
2.7	265.62311	265.62321	-0.4	$[M+2H]^{2+}$	$C_{21}H_{37}N_7O_7S$	Glutathione adduct

[d]Assignments are based on high mass accuracy (<3 ppm root-mean-square error).

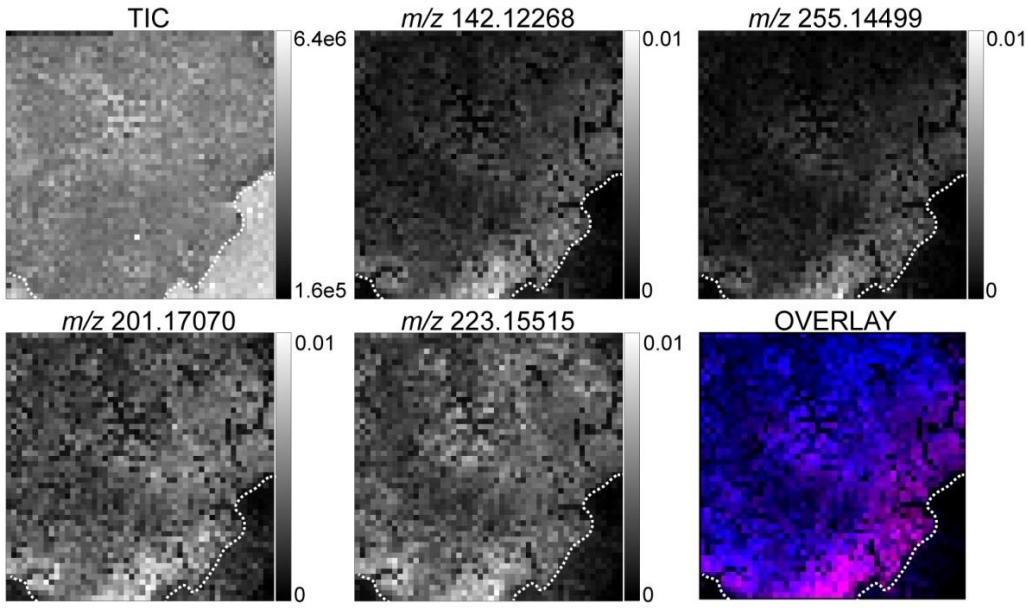

Figure 3. AP-SMALDI MSI of a tumor tissue section showing the distribution of pimonidazole-derived ions. A different distribution was observed for *m/z* 201.17070 and 223.15515 as compared to the distribution for the parent compound at *m/z* 255.14499 and the side chain fragment at *m/z* 142.12268. The overlay of *m/z* 223.15515 (blue) and *m/z* 255.14499 (red) shows overlap of the two ions only at the border of the tissue section (pink). The intensity for each ion was normalized to the total ion count (TIC) per pixel.

Pimonidazole hydroxylamine is the four-electron reduction product that is the main reactive species that needs to be formed for thiol-binding to occur.[7,20,22] However, this molecule can rearrange to form hydroxy derivatives with the same elemental composition. The detection of *m/z* 241.2 in two major elution peaks points towards the detection of multiple species. The elution of hydroxylamine and hydroxyl derivatives in two chromatographic peaks has been previously reported for the 2-nitroimidazole benznidazole.[31,32]

Further reduction yields the six-electron reduction product of pimonidazole, which is an amine derivative (*m/z* 225.2). Interestingly, also a pimonidazole derivative at *m/z* 223.2 was detected in the tumor tissue samples from pimonidazole-injected mice. The LC separation increased the confidence of the identification of *m/z* 223 as a metabolite and not solely as a MALDI-induced species: *m/z* 223.2 had a different retention time (2.9 min) as compared to the unmodified pimonidazole compound (4.0 min). An ion with the same elemental composition is postulated to be the nitrenium intermediate that is responsible for binding to thiol groups.[22-24] However, a nitrenium ion is a highly reactive and short-lived species. The *m/z* 223.2 ion might therefore originate from a conjugate which undergoes in-source fragmentation regenerating the nitrenium ion or a structurally related species.[33] To our knowledge, an ion with this elemental composition has not been previously detected for pimonidazole or a 2-nitroimidazole analog.

The binding of reductively activated pimonidazole to a thiol-containing molecule was shown with the detection of an ion at *m/z* 265.6, which was assigned to a doubly charged pimonidazole adduct of glutathione. Its charge state was confirmed by detection of the ^{13}C and ^{34}S isotopic peaks at *m/z* +0.50168

and +0.99790, respectively. This glutathione adduct has previously been reported as a product of the *in vitro* reduction of misonidazole and *in vivo* reduction of benznidazole.[21,22,31]

As expected, several products of the hydrolytic fragmentation of reductively activated pimonidazole were found as well. Hydrolysis of a hydroxyl derivative yielded a dihydro dihydroxy compound (*m/z* 259.2).[22-24,32] This compound can fragment or react with other molecules, releasing glyoxal and a guanidine derivative (*m/z* 201.2).[34-36] The signals at *m/z* 271.2 and 273.2 were assigned to methoxy derivatives of pimonidazole.[31]

Pimonidazole metabolites as hypoxia markers in MSI. Most pimonidazole metabolites identified by LC-MS were detected in the AP-SMALDI imaging data, as determined by accurate mass matching. Figure 3 shows that a different distribution was observed for *m/z* 201.2 and 223.2 as compared to the distribution for the parent compound at *m/z* 255.1 and the side chain fragment at *m/z* 142.1.

To determine which pimonidazole metabolites are suitable markers for tumor hypoxia in MALDI-MSI, we compared for each metabolite the signal intensity and the contribution of MALDI fragments to the signal. For the MALDI-MSI data, only the derivatives at *m/z* 223.2 and 225.2 were detected, due to the lower sensitivity and mass resolution of the QTOF instrument as compared to the AP-SMALDI instrument. Nevertheless, when comparing *m/z* 223.2 with *m/z* 124.1 or 142.1, a similar difference in distribution was observed as determined by AP-SMALDI (Figure 2 and Figure 3).

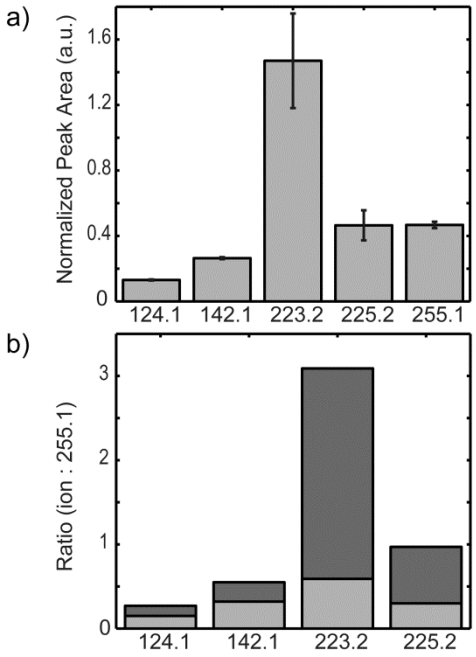

Figure 4. Pimonidazole derivative *m/z* 223.2 is detected with the highest intensity from tumor tissue. (a) MALDI-MSI detection of pimonidazole derivatives. Data are averaged for three tumors and shown as average ± standard deviation. (b) *m/z* 223.2 shows a five times higher detection after *in vivo* metabolism of pimonidazole as compared to detection from tissue homogenate mixed with unreacted pimonidazole (i.e. MALDI-induced fragmentation). Shown is the detection ratio for each ion as compared to *m/z* 255.1. Contribution of MALDI-induced fragmentation to the total signal is shown in light grey.

To determine the contribution of MALDI-induced fragmentation to the pimonidazole metabolite signals, 50 pmol pimonidazole was mixed with untreated tissue homogenate and measured with MALDI-MS. Pimonidazole derivative *m/z* 223.2 shows a five times higher detection after *in vivo* metabolism of pimonidazole as compared to the detection from tissue homogenate mixed with unreacted pimonidazole (Figure 4).

These results suggest that the ion at *m/z* 223.2 observed in tumor tissue from pimonidazole-injected animals can be mainly attributed to the pimonidazole metabolite. The pimonidazole derivative at *m/z* 223.2 could be easily detected in both the MALDI and AP-SMALDI imaging experiments. We therefore propose to use *m/z* 223.2 as hypoxia marker for mass spectrometric analysis of tumor tissue from pimonidazole-injected animals. All further analyses will focus on this pimonidazole derivative at *m/z* 223.2.

Verification of pimonidazole distribution with immunohistochemistry. Additional verification was performed with immunohistochemistry (IHC). IHC staining against pimonidazole is a widely used method for hypoxia detection.[14] Tissue sections adjacent to the sections used for mass spectrometric analysis were stained. The anti-pimonidazole stained images were co-registered with the MALDI-MSI data. Overlap between IHC and MSI detection of pimonidazole was determined by overlaying individual ion images and the anti-pimonidazole stained images. Figure 5 shows the results of this qualitative overlap analysis for one representative tumor. The darkest anti-pimonidazole stain was observed at the tumor boundary and at the border to necrotic regions. Pimonidazole metabolite *m/z* 223.2 co-localized with the marker detected by IHC mainly around the necrotic tumor core. The larger area stained positive for hypoxia by IHC might be explained by the higher sensitivity of IHC as compared to MSI. The detected species are also different: IHC detects pimonidazole protein adducts and MSI detects unbound pimonidazole metabolites.

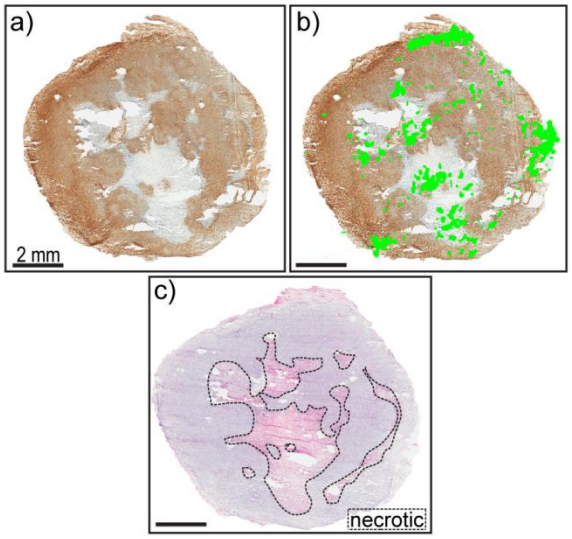

Figure 5. IHC detection of pimonidazole. (a) Distribution of hypoxic regions. Brown tissue staining is indicative of pimonidazole binding (b) Co-registration of a normalized and thresholded MS image of pimonidazole metabolite *m/z* 223.2 (green) from an adjacent tissue section. (c) H&E stained adjacent tissue section.

In addition, adjacent tissue sections were co-registered for the analysis and did not perfectly overlap. The use of an MSI-based hypoxia marker makes co-registration unnecessary, and thus avoids a potentially error-introducing step. Figure S-2 in the Supporting Information shows these data for all three tumors.

Correlation of the pimonidazole metabolite *m/z* 223.2 with endogenous lipids and metabolites. Hypoxic regions in MDA-MB-231 breast tumor xenografts were identified by means of the hypoxic pimonidazole metabolite *m/z* 223.2. We performed correlation analysis to identify biomolecules that are spatially correlated with these hypoxic regions. All three tumors showed a highly similar correlation pattern as determined by Pearson's correlation. The strongest correlations were identified for three low molecular weight ions at *m/z* 137.1, 160.1 and 204.1 (Figure 6). These ions show indeed a similar distribution as compared to the pimonidazole metabolite *m/z* 223.2 (insets Figure 6). Accurate mass measurements and on-tissue MS/MS fragmentation analyses identified these ions as 1-methylnicotinamide $[M]^+$ for *m/z* 137.1 and acetylcarnitine $[M+H]^+$ for *m/z* 204.1. The ion at *m/z* 160.1 (elemental composition $C_8H_{18}NO_2$) remains so far unidentified. Figure S-3 in the Supporting Information shows the fragmentation spectra for these ions.

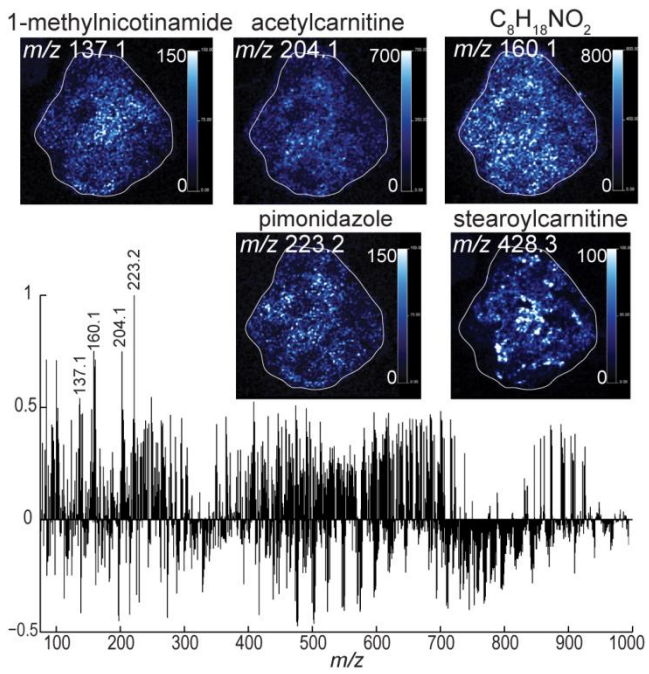

Figure 6. Correlation of *m/z* 223.2 with other *m/z* features as determined by Pearson's correlation. 1-methylnicotinamine, $C_8H_{18}NO_2$ and acetylcarnitine were found to be highly correlated with *m/z* 223.2. Data are shown for one representative tumor section.

Elevated levels of 1-methylnicotinamide were previously found in human cell lines overexpressing nicotinamide N-methyltransferase using untargeted LC-MS/MS analysis.[37] Nicotinamide N-methyltransferase catalyzes the transfer of a methyl group from S-adenosyl-L-methionine to nicotinamide, generating S-adenosylhomocysteine and 1-methylnicotinamide. This enzyme is overexpressed in several cancer types and is known to support tumorigenesis.[38,39] A high expression of nicotinamide N-methyltransferase has been reported for the MDA-MB-231 breast cancer cell line used as orthotopic xenograft model in this study.[40] It was previously reported that nicotinamide N-methyltransferase is involved in the regulation of protein methylation in cancer cells, whereby 1-methylnicotinamide functions as a sink for methylation units.[37]

We have identified the ion at *m/z* 204.1 as the protonated ion of acetylcarnitine. A previous MALDI-MSI study using the same breast tumor xenograft model identified two acylcarnitines that localized to hypoxic tumor regions, namely palmitoylcarnitine and stearoylcarnitine.[41] Stearoylcarnitine at *m/z* 428.3 was also positively correlated with pimonidazole in this study (Figure 6). Carnitine and acetylcarnitine are involved in the mitochondrial metabolism of acetyl coenzyme A (acetyl-CoA). Acetyl-CoA is converted to CoA and acetylcarnitine in the presence of carnitine.[42] The free CoA can then be used for fatty acid oxidation and in the citric acid cycle. Hypoxia is associated with a perturbation of CoA homeostasis and an increase in the ratio between acylcarnitines and free carnitine.[43]

CONCLUSIONS

With MSI, the distribution of a wide variety of biomolecules can be studied. Ideally, these distributions are directly correlated with tissue regions of interest. However, the markers that delineate these tissue regions can typically only be studied with other imaging techniques, such as IHC. We have used the exogenous marker pimonidazole for direct detection of hypoxic tissue regions in a breast tumor xenograft model with MALDI-MSI, thereby avoiding the co-registration of MSI data with other imaging data.

A MALDI-MSI approach is presented that combines the detection of pimonidazole and a hypoxic pimonidazole metabolite with the multiplexing capabilities of the technique. We have used pimonidazole derivative *m/z* 223.2 to image hypoxic tissue regions and their associated lipids and small molecules. Several endogenous species localized to hypoxic tissue regions as defined by this hypoxic pimonidazole metabolite. Interestingly, the identified species are known to be involved in hypoxia or metabolic reprogramming in cancer, although their specific roles remain to be elucidated. Ultimately, endogenous molecules might be identified that can serve as hypoxia markers for MSI.

Pimonidazole is a widely used marker of tissue hypoxia. We expect that the presented MALDI-MSI approach is also applicable to other tissues from pimonidazole-injected animals or humans.

ASSOCIATED CONTENT

Supporting Information

Supporting Information Available: additional Materials and Methods and Supporting Figures S1-S3. This material is available free of charge via the Internet at http://pubs.acs.org.

AUTHOR INFORMATION

Corresponding Authors

*Ron M.A. Heeren. Tel:+31-433881499. E-mail: r.heeren@maastrichtuniversity.nl

*Kristine Glunde. Tel: +1 (410)-614-2705. Fax: +1 (410)-614-1948. E-mail: kglunde@mri.jhu.edu.

Author Contributions

NEM conceived and carried out experiments, analyzed data, and wrote the manuscript. MC and ARI performed the animal experiments and stainings. LJ analyzed data and assisted in data interpretation. HP performed the LC-MS experiments. ARO, DRB and RMAH worked on the AP-SMALDI experiments. RMAH and KG supervised the project and assisted in writing of the manuscript. All authors approved the final version of the manuscript.

Notes

The authors declare no competing financial interest.

ACKNOWLEDGMENTS

This work is part of the research program of the Foundation for Fundamental Research on Matter (FOM) which is financially supported by the Netherlands Organization for Fundamental Research (NWO). NEM and RMAH acknowledge financial support from the Dutch national program COMMIT. This work was in part supported by the National Institutes of Health (NIH) grants R01 CA134695, R01 CA154725, and P50 CA103175. The authors thank Alfons Hester and Ivo Klinkert for providing support with the Mirion software and Berta Cillero Pastor for assisting with the metabolite experiments. The authors gratefully acknowledge Deutsche Forschungsgemeinschaft (DFG, Sp 314/13-1) for the financial support.

REFERENCES

(1) Rademakers, S. E.; Span, P. N.; Kaanders, J. H.; Sweep, F. C.; van der Kogel, A. J.; Bussink, *J. Mol Oncol* **2008**, 2, 41-53.

(2) Hockel, M.; Vaupel, P. *J Natl Cancer Inst* **2001**, 93, 266-276.

(3) Krohn, K. A.; Link, J. M.; Mason, R. P. *J Nucl Med* **2008**, 49 Suppl 2, 129S-148S.

(4) Adams, A.; van Brussel, A. S.; Vermeulen, J. F.; Mali, W. P.; van der Wall, E.; van Diest, P. J.; Elias, S. G. *BMC Cancer* **2013**, 13, 538.

(5) Varghese, A. J.; Gulyas, S.; Mohindra, J. K. *Cancer Res* **1976**, 36, 3761-3765.

(6) Chapman, J. D.; Franko, A. J.; Sharplin, J. *Br J Cancer* **1981**, 43, 546-550.

(7) Varghese, A. J.; Whitmore, G. F. *Cancer Res* **1980**, 40, 2165-2169.

(8) Raleigh, J. A.; Miller, G. G.; Franko, A. J.; Koch, C. J.; Fuciarelli, A. F.; Kelly, D. A. *Br J Cancer* **1987**, 56, 395-400.

(9) Sobhanifar, S.; Aquino-Parsons, C.; Stanbridge, E. J.; Olive, P. *Cancer Res* **2005**, 65, 7259-7266.

(10) Huang, T.; Civelek, A. C.; Li, J.; Jiang, H.; Ng, C. K.; Postel, G. C.; Shen, B.; Li, X. F. *J Nucl Med* **2012**, 53, 1262-1268.

(11) Rompp, A.; Guenther, S.; Takats, Z.; Spengler, B. *Anal Bioanal Chem* **2011**, 401, 65-73.

(12) Thomas, A.; Charbonneau, J. L.; Fournaise, E.; Chaurand, P. *Anal Chem* **2012**, 84, 2048-2054.

(13) Rompp, A.; Spengler, B. *Histochem Cell Biol* **2013**, 139, 759-783.

(14) Varia, M. A.; Calkins-Adams, D. P.; Rinker, L. H.; Kennedy, A. S.; Novotny, D. B.; Fowler, W. C.; Raleigh, J. A. *Gynecol Oncol* **1998**, 71, 270-277.

(15) Raleigh, J. A.; Chou, S. C.; Arteel, G. E.; Horsman, M. R. *Radiat Res* **1999**, 151, 580-589.

(16) Gross, M. W.; Karbach, U.; Groebe, K.; Franko, A. J.; Mueller-Klieser, W. *Int J Cancer* **1995**, 61, 567-573.

(17) Arteel, G. E.; Thurman, R. G.; Yates, J. M.; Raleigh, J. A. *Brit J Cancer* **1995**, 72, 889-895.

(18) Chou, S. C.; Azuma, Y.; Varia, M. A.; Raleigh, J. A. *Br J Cancer* **2004**, 90, 728-735.

(19) Arteel, G. E.; Thurman, R. G.; Raleigh, J. A. *Eur J Biochem* **1998**, 253, 743-750.

(20) Varghese, A. J.; Whitmore, G. F. *Chem Biol Interact* **1981**, 36, 141-151.

(21) Varghese, A. J. *Biochem Biophys Res Commun* **1983**, 112, 1013-1020.

(22) Varghese, A. J.; Whitmore, G. F. *Chem Biol Interact* **1985**, 56, 269-287.

(23) McClelland, R. A.; Panicucci, R.; Rauth, A. M. *J Am Chem Soc* **1985**, 107, 1762-1763.

(24) Bolton, J. L.; Mcclelland, R. A. *J Am Chem Soc* **1989**, 111, 8172-8181.

(25) Raleigh, J. A.; Koch, C. J. *Biochem Pharmacol* **1990**, 40, 2457-2464.

(26) Chughtai, K.; Jiang, L.; Greenwood, T. R.; Klinkert, I.; van Hove, E. R. A.; Heeren, R. M. A.; Gunde, K. *Anal Chem* **2012**, 84, 1817-1823.

(27) Koestler, M.; Kirsch, D.; Hester, A.; Leisner, A.; Guenther, S.; Spengler, B. *Rapid Commun Mass Spectrom* **2008**, 22, 3275-3285.

(28) Paschke, C.; Leisner, A.; Hester, A.; Maass, K.; Guenther, S.; Bouschen, W.; Spengler, B. *J Am Soc Mass Spectrom* **2013**, 24, 1296-1306.

(29) Eijkel, G. B.; Kaletas, B. K.; van der Wiel, I. M.; Kros, J. M.; Luider, T. M.; Heeren, R. M. A. *Surf Interface Anal* **2009**, 41, 675-685.

(30) Jiang, L.; Greenwood, T. R.; van Hove, E. R.; Chughtai, K.; Raman, V.; Winnard, P. T., Jr.; Heeren, R. M.; Artemov, D.; Glunde, K. *Nmr Biomed* **2013**, 26, 285-298.

(31) Trochine, A.; Creek, D. J.; Faral-Tello, P.; Barrett, M. P.; Robello, C. *PLoS Negl Trop Dis* **2014**, 8, e2844.

(32) Hall, B. S.; Wilkinson, S. R. *Antimicrob Agents Chemother* **2012**, 56, 115-123.

(33) Masaki, Y.; Shimizu, Y.; Yoshioka, T.; Tanaka, Y.; Nishijima, K.; Zhao, S.; Higashino, K.; Sakamoto, S.; Numata, Y.; Yamaguchi, Y.; Tamaki, N.; Kuge, Y. *Sci Rep* **2015**, 5, 16802.

(34) Varghese, A. J.; Whitmore, G. F. *Cancer Res* **1983**, 43, 78-82.

(35) Heimbrook, D. C.; Sartorelli, A. C. *Mol Pharmacol* **1986**, 29, 168-172.

(36) Raleigh, J. A.; Liu, S. F. *Biochem Pharmacol* **1983**, 32, 1444-1446.

(37) Ulanovskaya, O. A.; Zuhl, A. M.; Cravatt, B. F. *Nat Chem Biol* **2013**, 9, 300-306.

(38) Tang, S. W.; Yang, T. C.; Lin, W. C.; Chang, W. H.; Wang, C. C.; Lai, M. K.; Lin, J. Y. *Carcinogenesis* **2011**, 32, 138-145.

(39) Wu, Y.; Siadaty, M. S.; Berens, M. E.; Hampton, G. M.; Theodorescu, D. *Oncogene* **2008**, 27, 6679-6689.

(40) Zhang, J.; Wang, Y. Z.; Li, G. L.; Yu, H. T.; Xie, X. Y. *PLoS One* **2014**, 9(2): e89202.

(41) Chughtai, K.; Jiang, L.; Greenwood, T. R.; Glunde, K.; Heeren, R. M. *J Lipid Res* **2013**, 54, 333-344.

(42) Kerner, J.; Hoppel, C. *Biochim Biophys Acta* **2000**, 1486, 1-17.

(43) Wainwright, M. S.; Kohli, R.; Whitington, P. F.; Chace, D. H. *Stroke* **2006**, 37, 524-530.

Insert Table of Contents artwork here